








# Mitigating modal noise in multimode circular fibres by optical agitation using a galvanometer

Supriyo Ghosh <sup>1</sup>★, Chantira Boonsri <sup>2</sup>, William Martin,<sup>1</sup> Hugh R. A. Jones <sup>1</sup>,  
Piyamas Choochalem <sup>2</sup>, Sarah Usher,<sup>3</sup> Stephanos Yerolatsitis <sup>4,5</sup>, Thomas Wocial <sup>1</sup>  
and Thomas Wright <sup>4</sup>

<sup>1</sup>Centre for Astrophysics Research, Department of Physics, Astronomy and Mathematics, University of Hertfordshire, Hatfield, Hertfordshire AL10 9AB, UK

<sup>2</sup>National Astronomical Research Institute of Thailand (NARIT), Don Kaeo, Mae Rim District, Chiang Mai 50180, Thailand

<sup>3</sup>Thorlabs Vytran Europe, 2 Kew Court, Exeter EX2 5AZ, UK

<sup>4</sup>Centre for Photonics and Photonic Materials, Department of Physics, University of Bath, Claverton Down, Bath BA2 7AY, UK

<sup>5</sup>University of Central Florida, 4000 Central Florida Blvd. Orlando, Florida, FL 32816, USA

Accepted 2023 December 28. Received 2023 November 22; in original form 2023 September 11

## ABSTRACT

Modal noise appears due to the non-uniform and unstable distribution of light intensity among the finite number of modes in multimode fibres. It is an important limiting factor in measuring radial velocity precisely by fibre-fed high-resolution spectrographs. The problem can become particularly severe as the fibre's core become smaller and the number of modes that can propagate reduces. Thus, mitigating modal noise in relatively small core fibres still remains a challenge. We present here a novel technique to suppress modal noise. Two movable mirrors in the form of a galvanometer re-image the mode-pattern of an input fibre to an output fibre. The mixing of modes coupled to the output fibre can be controlled by the movement of mirrors applying two sinusoidal signals through a voltage generator. We test the technique for four multimode circular fibres: 10 and 50  $\mu\text{m}$  step-index, 50  $\mu\text{m}$  graded-index, and a combination of 50  $\mu\text{m}$  graded-index and 5:1 tapered fibres (GI50t). We present the results of mode suppression both in terms of the direct image of the output fibre and spectrum of white light obtained with the high-resolution spectrograph. We found that the galvanometer mitigated modal noise in all the tested fibres, but was most useful for smaller core fibres. However, there is a trade-off between the modal noise reduction and light-loss. The GI50t provides the best result with about 60 per cent mitigation of modal noise at a cost of about 5 per cent output light-loss. Our solution is easy to use and can be implemented in fibre-fed spectrographs.

**Key words:** Instrumentation – Spectrograph – Optical Fibres – Modal Noise – Galvanometer.

## 1. INTRODUCTION

Measuring radial velocity (RV) is one of the key techniques to detect and characterize extrasolar planets. To measure RV accurately, high-resolution spectrographs (for instance, HARPS: Mayor et al. 2003, HPF: Mahadevan et al. 2012, ESPRESSO: Mégevand et al. 2012, CARMENES: Quirrenbach et al. 2012, PARAS: Chakraborty et al. 2014, SPIRou: Artigau et al. 2014, NIRPS: Bouchy et al. 2017, NEID: Allen et al. 2018, and MAROON-X: Seifahrt et al. 2018) have been deployed on the different telescopes. However, the current generation of RV instruments cannot achieve the required precision ( $10 \text{ cm s}^{-1}$ ) to detect earth-like exoplanets orbiting sun-like (G-type) stars (Fischer et al. 2016). To achieve such precision, it is important to maintain prolonged and extreme stability and accurate wavelength calibration of the instrument. A significant obstacle lies in stabilizing the instrument's illumination, particularly as its profile changes with varying illumination conditions (Hunter & Ramsey 1992).

As a remedy, the current generation of seeing-limited RV spectrographs use multimode (MM) fibres, in general, to feed the light to the spectrograph from the telescope (Hill et al. 1980; Avila 1988). In addition, utilizing the fibre effectively decouples the physical link between the instrument and telescope's focal point, resulting in a substantial improvement in detection sensitivity. A large core MM fibre is generally used to maximize the light gathered. However, due to the finite modes in MM fibres and the potential for subtle illumination changes, there is a concern about signal distortion by the interference of the modes as they propagate along the fibre, leading to the characteristic speckle associated with modal noise (Mickelson & Weierholt 1983). Modal noise, characterized by this speckle pattern, arises from the interference of the finite modes in the fibres. The amount of distortion depends on the wavelength of light, core diameter, refractive index, state of the fibre, and fibre coupling and is also sensitive to environmental variation such as temperature (Petersburg et al. 2018). Furthermore, the term modal noise was introduced as the effect that distorts the signal and appears as amplitude modulation (Epworth 1978). When using a fibre to feed a spectrograph, modal noise can also be observed as focal ratio degradation (Ramsey 1988). Recent studies found

\* E-mail: [supriyoani89@gmail.com](mailto:supriyoani89@gmail.com)

that suitable tapered graded-index (GI) fibres provide an alternative way for efficient focal ratio reduction in fibre-fed spectrographs (Choochalerms et al. 2021, 2023). Floris et al. (2020) showed that modal noise in GI MM fibres can be reproduced by geometrical-optics-based models. The role of modal noise on the spectrograph performance was extensively investigated in Oliva et al. (2019) as it depends on the illumination of the source and in some cases the modal noise is negligible. None the less, the modal noise has an adverse impact on the precision of RV measurements when left unmitigated (Mahadevan et al. 2014).

Over the years, various techniques have been proposed for mitigating modal noise in MM fibres, including single-mode scramblers (Spronck et al. 2012, 2013), double-mode scramblers (Hunter & Ramsey 1992; Spronck et al. 2013, 2015; Roy et al. 2014; Halverson et al. 2015a; Oliva et al. 2019), rotating double scramblers (Raskin et al. 2020), dynamical diffusers with integrating sphere and rotating mirror (Mahadevan et al. 2014), hand agitation (McCoy et al. 2012; Mahadevan et al. 2014), mechanical agitators (McCoy et al. 2012; Petersburg et al. 2018; Oliva et al. 2019), and photonic lanterns (Leon-Saval et al. 2005; Birks et al. 2015; Yerolatsitis et al. 2017; Pike et al. 2020). Nevertheless, the suppression of modal noise in MM fibres continues to pose a challenge, particularly for fibres with relatively small core diameters.

Due to modal noise issues in MM fibres, single-mode fibres have been proposed as an alternative for next-generation RV spectrographs (Crepp 2014; Blake et al. 2015; Crepp et al. 2016; Schwab et al. 2016). Light in single-mode fibres propagates in a single spatial mode. This not only eliminates the modal noise issue encountered when using MM fibres but also enhances the stability of the output illumination. None the less, the performance of single-mode fibre spectrographs is limited (Halverson et al. 2015b), due to the narrow operational bandwidth in the optical range (typically 100–200 nm in the visible, Petersburg et al. 2018) and the interaction between the fundamental polarization modes (Monerie & Jeunhomme 1980).

In this paper, we describe an off-the-shelf, easy-to-use technique to mitigate modal noise for small core (10  $\mu\text{m}$ ) MM fibres. We have investigated the effectiveness of our solution on a high-resolution spectrograph, EXO-planet high-resolution SPECTrograph (EXOhSPEC, Kawinkij et al. 2019; Lhospipe et al. 2019; Jones et al. 2021) using step-index (SI), GI, and tapered GI optical fibres. The paper is structured as follows: Modal noise on EXOhSPEC is presented in Section 2. The experimental set-up for our study is described in Section 3, while Section 4 covers our results and discussion. Finally, the summary of the study is presented in Section 5.

## 2. MODAL NOISE ON EXOHSPEC WITH FIBRES

EXOhSPEC is an actively controlled fibre-fed double-pass optical spectrograph with a spectral resolution of  $>70\,000$  and is designed for 10  $\mu\text{m}$  core fibre with 0.10 numerical aperture. It was built principally from off-the-shelf components such as a collimator/camera lens, cross-dispersing prism, grating, and Complementary Metal Oxide Semiconductor (CMOS) detector and has overall dimensions of approximately 30  $\times$  40 cm  $\times$  50 cm. The main instrument is currently under development for the 2.4 m *Thai National Telescope* at the National Astronomical Research Institute of Thailand. A prototype of the instrument is at the University of Hertfordshire (UH), United Kingdom, where new techniques are tested to improve the performance and stabilization of the spectrograph. The aim of this project is to develop an efficient high-resolution spectrograph

for exoplanet study as well as to reduce the size and cost with only a modest impact on the performance.

A schematic diagram of the spectrograph is shown inside a rectangular box in Fig. 1. Additional details on the spectrograph can be found in Jones et al. (2021). As mentioned the EXOhSPEC is a fibre-fed spectrograph, the fibre link is required in order to achieve the high-precision performance. However, modal noise can limit the optimization of a fibre-feeding system for astronomical observations.

As the instrument is designed for a 10  $\mu\text{m}$  core fibre, a 10  $\mu\text{m}$  core Thorlabs SI MM fibre was set up in the first place for data acquisition. The significant amount of modal noise on the UH prototype was evident in our previous study (Jones et al. 2021). The extracted spectrum of continuum frames showed apparently periodic features of substantial strength. The strength of wavy spectral features was found to decrease as measurements shifted from redder (900 nm) to bluer (460 nm) wavelength regimes. This is because the number of modes at the bluer end is relatively higher than the redder end and thus the modes are averaged out at the bluer end. This observation agrees well with the previous studies (see Baudrand & Walker 2001).

A re-set-up of the experiment was required to test the impact of fibre movement on modal noise. For that, the fibre was disturbed by manual shaking, stretching and squeezing as shown in Fig. 2. The spectrum of the white light was obtained through the disturbed fibre. For a preliminary assessment, the spectrum of white light was extracted using MaxIm DL.<sup>1</sup> The average counts of a user-defined box with a height (i.e. along the dispersion direction) of 4000 pixels and a width (i.e. along the cross-dispersion direction) of 50 pixels around a certain order are adopted for the spectrum extraction. The extracted spectrum is then fitted with a 4th order polynomial for normalization. The normalized spectra are displayed in Fig. 3 for different fibre conditions. Looking at the spectra, we can see that the spectrum changes with the change in the fibre's state. In fact, the overall pattern of modes between the same fibres taken after set-up on different days is larger than differences that we can induce in the fibres by shaking, squeezing or stretching. To make the speckle pattern stable and suppress this modal noise, we investigated the use of optical reimaging agitation to mix the modes using a galvanometer as demonstrated in the following section.

## 3. EXPERIMENTAL SET-UP

We investigated our galvanometer-based technique on the UH prototype of the spectrograph with fibres of different core sizes and refractive index profiles. The core size and refractive index profile of a fibre defines the number of modes, hence the amount of modal noise for a fixed illumination. Moreover, we are interested in testing both MM SI and GI fibres. SI fibres are traditionally used in the fibre-fed spectrographs (e.g. Ishizuka et al. 2018; Petersburg et al. 2018) because of its relatively high transmission in the blue region. However, with GI fibre, refocusing of the signal within the core is increased because of the parabolic refractive index profile. Also, the pulse dispersion for a given distance is smaller in GI fibre than SI fibre. In addition, we adopted conventional circular core fibres for our experiment instead of other types of fibre such as rectangular and octagonal core fibres as our main objective is to test the effectiveness our method in suppressing modal noise.

<sup>1</sup><https://diffractionlimited.com/product/maxim-dl/>

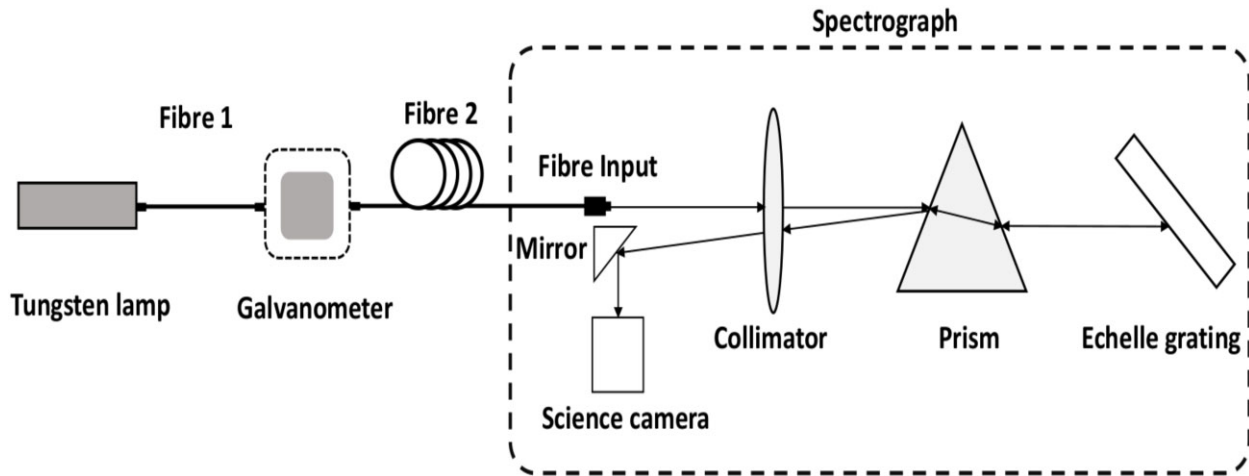


**Figure 1.** Schematic layout of the experimental set-up to investigate the impact of modal noise on the spectra. The optical diagram of the EXOhSPEC spectrograph is also presented inside the box. The figure depicts the experimental set-up where the galvanometer was implemented to mitigate the modal noise. Two identical fibres (Fibre 1 and Fibre 2) were in use. Fibre 1 was coupled between the Tungsten lamp (a white light source) and the input of the galvanometer. The galvanometer randomizes the incoming modes and collimates light onto Fibre 2. Fibre 2 was from the output of the galvanometer to the spectrograph. Spectrograph is in use to obtain high-resolution spectra of white light. This set-up was termed the ‘GAL ON’ condition. In the ‘GAL OFF’ condition, Fibre 2 was used to feed the spectrograph directly with the white light but without the galvanometer.

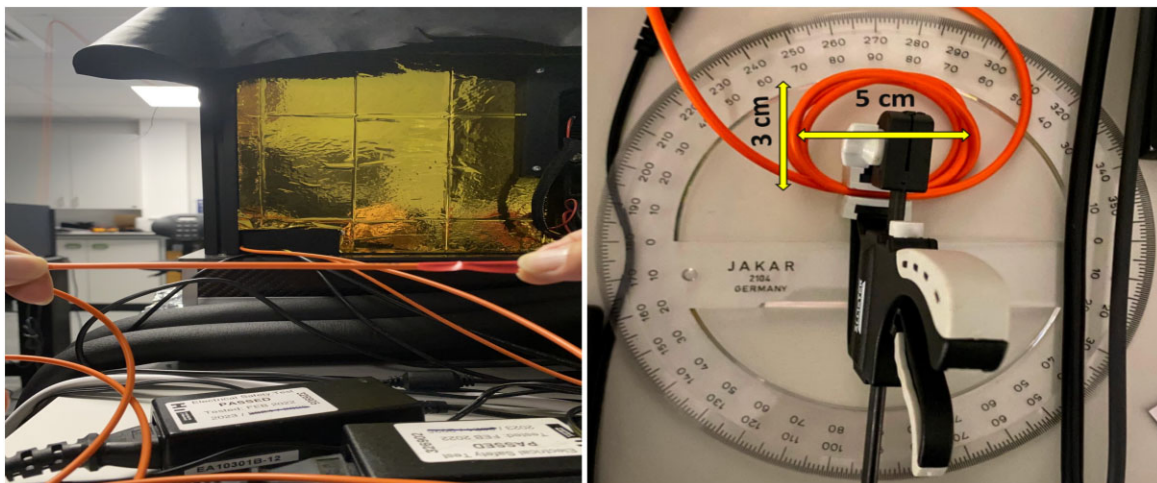


**Figure 2.** Illustration of disturbing (left panel: stretching and right panel: squeezing) the fibre to study the modal noise on EXOhSPEC. The stretching and squeezing were performed by pulling the fibre in the opposite direction and by rolling the fibre with a diameter of 3 cm, respectively. A 10  $\mu\text{m}$  core 0.1 numerical aperture MM SI fibre was used for this test.

### 3.1 Description of galvanometer

The galvanometer system consists of a Thorlabs GVSX02 dual-axis galvo, and two fibre collimators (TC06FC-633). There are two movable flat mirrors in the galvanometer, Mirror 1 and Mirror 2. For detailed configuration of the galvanometer, we refer to the catalogue. The reflectivity of two mirrors is 95 per cent<sup>2</sup> at 635 nm. Fig. 4 presents a schematic of the galvanometer set-up. One end of Fibre 1 is connected to a white light source. The other end is connected to the input fibre coupler of the galvanometer. Light from the input fibre, Fibre 1, is collimated by the first collimator, directed to the first movable mirror Mirror 1, and reflected towards the second movable

mirror Mirror 2. The reflected light from the Mirror 2 is refocused to the input of Fibre 2 by the output fibre collimator. Fibre 2 is connected to the spectrograph.

Both mirrors are mounted on motorized rotating mounts. Using this configuration we are able to move the two mirrors independently. The mode pattern from Fibre 1 is moved in X and Y and is collimated to focus on Fibre 2. The modes of Fibre 2 are excited randomly and hence, the output illumination pattern varies continuously throughout an appropriately long integration time. As a result, the speckle pattern is averaged out efficiently at the exit of Fibre 2. Thus, two movable mirrors mix the modes before recoupling the light from the input to the output fibre.

The movement of the mirrors can be controlled by applying sinusoidal signals on two channels (CH 1 and CH 2) of a voltage generator. Controlling the frequency and amplitude of the signal, we

<sup>2</sup><https://www.thorlabs.com/catalogpages/Obsolete/2023/GVS302.pdf>

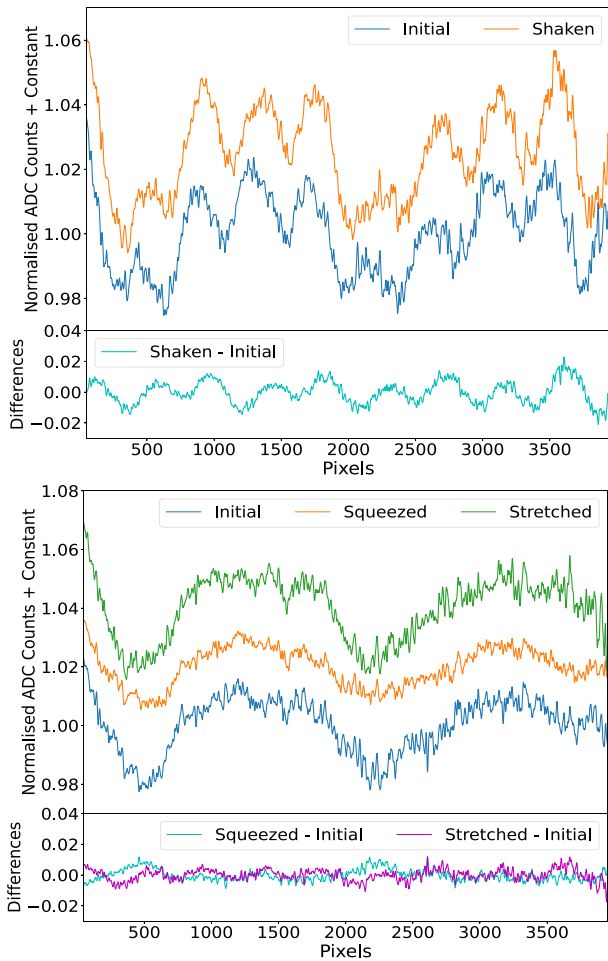


**Figure 3.** Illustration of the modal noise impact on the white light spectra when a 10  $\mu\text{m}$  SI fibre was shaken (upper panel) as well as squeezed and stretched (lower panel). The data for the two panels were obtained for the same fibre after set-up on different dates.

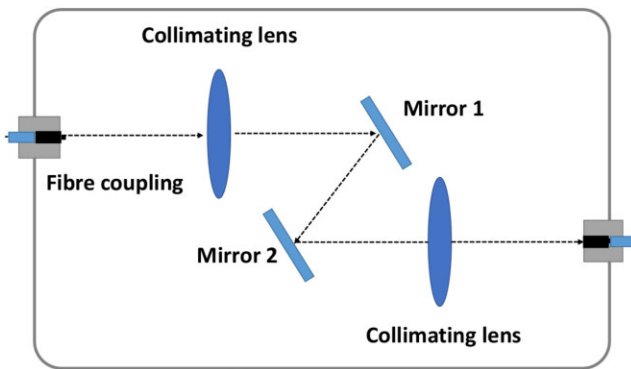


**Figure 4.** Schematic layout of the galvanometer used for suppressing the modal noise. Two motorized rotating flat mirrors that are used to mix the modes can be controlled by altering the amplitude and voltage of the applied signal to each channel independently through a voltage generator.

can control the movement of mirrors, hence the mixing of modes. CH 1 controls the Y-axis movement of the Mirror 1 and CH 2 controls the X-axis movement of the Mirror 2.

The optimum amplitudes and frequencies for operating the galvanometer were explored and this is discussed in Section 4. Before setting up the galvanometer the two mirrors were optimally aligned using a fibre coupled laser by applying a small DC offset voltage through the voltage generator to optimize the output for a given input to the galvanometer. We set the frequency and amplitude of the signal to each of the mirrors at 1 Hz and 1 mV, respectively, and changed the DC offset voltage to find optimum settings of the galvanometer output using a power meter. The DC offset voltages for the maximum throughput power were found to be  $-65$  mV and 1.48 V for CH 1 and CH 2, respectively. We repeated the test for different values of frequencies and amplitudes and found that the DC offset voltages remained the same. This indicates that there is no dependence of the applied frequencies and amplitudes on the DC offset voltage. Once the DC offset voltage is fixed at the beginning of the experiment, it remains the same during the experiment. Furthermore, we have noticed no notable change in DC offset value in our day-to-day experiments.

We determined the angle of rotation of two mirrors due to the applied signals to the voltage generator by removing the collimators. We calculated the angle of rotation of the two mirrors in response to the signals applied to the voltage generator. The rotation of the mirrors due to applied voltage at CH 1 and CH 2 to be  $36.6$  and  $51.8$   $\mu\text{rad mV}^{-1}$ , respectively. Translating the rotation of the mirrors into the movement on the output fibre, we obtained  $0.5$  and  $1.3$   $\mu\text{m mV}^{-1}$  along X and Y-axes, respectively. For the application of 1 mV to each of the mirrors, the focal spot of the output beam would typically move  $\sim 1.4$   $\mu\text{m}$ .

### 3.2 Data acquisition

We performed our experiment with four circular MM fibres. As mentioned above, the instrument is designed for a 10  $\mu\text{m}$  core input fibre with 0.10 numerical aperture. We tested both 10  $\mu\text{m}$  core SI (SI10) as well as GI fibres. A SI10 is commercially available, however, a 10  $\mu\text{m}$  core GI fibre is not. Thus, we connected a 50  $\mu\text{m}$  GI fibre with a custom 5:1 tapered fibre (GI50t) i.e. waist of the tapered fibre has a 10  $\mu\text{m}$  core and so should behave approximately as a 10  $\mu\text{m}$  core GI fibre. The tapering process was performed on a Thorlabs Vytran GPX3400 Glass Processor. The tapered fibre generally converts the beam diameter of an input beam to a small diameter and rejects relatively high-order modes. We refer to Choochalerm et al. (2021, 2023) for details on the transmission properties of tapered optical fibres. Additionally, we investigated commercially available 50  $\mu\text{m}$  SI (SI50) and 50  $\mu\text{m}$  GI fibres for comparison purposes. We did not test fibres having larger core diameters than 50  $\mu\text{m}$  core as the modal noise reduces with the enlargement of fibre core size. The additional details of the fibres are listed in Table 1. A white light source (tungsten lamp—Thorlabs SLS201L/M) was used to illuminate the fibre on test (see Fig. 1). Following the procedure described below, we were able to test the performance of our method.

(i) GAL ON: Two identical fibres, namely Fibre 1 and Fibre 2, were used. Fibre 1 established a connection between the white light source and the input of the galvanometer. Fibre 2 connected the output of the galvanometer to the spectrograph as shown in Fig. 1. The modes of second fibre were being agitated by the galvanometer.

**Table 1.** Details on the adopted fibres for investigation.

Fibre type	Core size	Numerical aperture	Number of modes <sup>a</sup>	Manufacturer	Part number
SI50	50 $\mu\text{m}$	0.22	988	Thorlabs	FG050LGA
GI50	50 $\mu\text{m}$	0.20	816	Thorlabs	GIF50E
SI10	10 $\mu\text{m}$	0.1	8	Thorlabs	FG010LDA
GI50t	10 $\mu\text{m}$	0.2	16	University of Bath <sup>b</sup>	Custom

Notes.

<sup>a</sup>The length of each fibre is 5 m. The number of modes for each fibre was estimated using equation (1) of Petersburg et al. (2018) at 0.7  $\mu\text{m}$ .

<sup>b</sup>The fibre used for tapering was from University of Bath and it was tapered by Thorlabs Vytran Automated glass processing workstation (GPX3400).

(ii) GAL OFF: No galvanometer was inserted into the light path. Fibre 1 is removed and Fibre 2 was connected from the white light source directly to the spectrograph. There was no agitation in this case.

The goal of our two measurement setups was to compare the modal noise between sets of spectra obtained both with and without agitation and thereby verify the effectiveness of our method. The typical exposures were 0.4 s for 50  $\mu\text{m}$  fibres (SI50 and GI50) and 5 and 10 s for GI50t and SI10, respectively.

### 3.3 Spectrum extraction

We performed data analysis in Python, correcting the raw data set of the white light (image frames) for bias, dark, and flat before extracting its spectra. We utilized five bias (dark) frames for bias (dark) correction, respectively. We median combined the images on a pixel-by-pixel basis and subtracted them from the image frames. We obtained five frames of white light for flat correction at the start of each day's data acquisition. After bias and dark corrections, we median combined these frames on a pixel-by-pixel basis. We smoothed the combined flat frame by implementing a median filter. We then divided it by its smoothed version for normalization. We used the normalized flat frame for flat correction. Finally, we used the flat-corrected frame for spectrum extraction. We extracted the spectrum of a particular order, which was at the redder side of the detector, using the SpectrumExtractor tool.<sup>3</sup> The central wavelength of our selected order was approximately 700 nm. We picked up the order from the detector's redder side because of the relatively high throughput at this wavelength range. In addition, as the redder side propagates a relatively small number of modes, the impact of modal noise is higher on the redder side than the bluer. The same spectral order was used for all the investigated fibres for comparison purposes. A 4th order polynomial was found to be suitable to trace out the dispersion axis without overfitting the data. An aperture window of (−6, 6) pixels was specified for spectrum extraction via sum extraction.

### 3.4 Measurement of modal noise

To quantify the modal noise, various methods, for instance measuring the centroid drift and RV error (Mahadevan et al. 2014; Halverson et al. 2015a; Petersburg et al. 2018), signal-to-noise ratio (SNR, Oliva et al. 2019) and barycentre precision of spectral features (Pike et al. 2020) have been used. We used root-mean-square error (RMSE) to measure the modal noise. The extracted continuum lamp spectrum was divided by the fitted 4th order polynomial described above for

spectrum normalization. The deviation of the normalized spectrum from the ideal flat normalized continuum spectrum was measured by RMSE measurement using the following equation:

$$\text{RMSE}(y, \hat{y}) = \sqrt{\frac{\sum_{i=0}^{N-1} (y_i - \hat{y}_i)^2}{N}} \quad (1)$$

where  $y_i$  and  $\hat{y}_i$  are the ideal and observed normalized flat values for  $i$ th data point, respectively and  $N$  is the total number of data points. The amount of modal noise is proportional to the RMSE value. The limitation of using RMSE as a proxy for modal noise quantification is the SNR of the extracted spectrum. Thus, for our analysis, we used spectra from 100 pixels to 5000 pixels of an order because the SNR is higher and more uniform.

## 4. RESULTS AND DISCUSSION

### 4.1 Frequency of galvanometer agitation

In order to efficiently use the galvanometer the optimum frequency of operation was first evaluated. For that, the frequency of the voltage generator was varied from 1 to 600 Hz keeping the amplitude fixed at a certain value for all fibres investigated as shown in Fig. 5. Based on the size of the core of the fibre, we carried out our experiment with different values of amplitude. We carried out the test at two amplitudes: 1 and 60 mV for SI50, GI50, and GI50t, and 1 and 20 mV for SI10. We extracted the spectrum for an order in each case as mentioned in Section 3.3 and evaluated RMSEs following the approach described in Section 3.4. We found no clear evidence of frequency dependence (between 1 and 600 Hz) on the RMSE measurement for any of the fibres. None the less, applied frequencies of 89 Hz to Mirror 1 (CH 1) and 97 Hz to Mirror 2 (CH 2) satisfying the condition for fibre agitation frequency proposed by Baudrand & Walker (2001). It states that the agitation frequency should be much greater than  $1/\tau$ , where  $\tau$  is the exposure time. Our values of integration are 0.4–10 s, so values of frequencies (89 and 97 Hz) always exceed  $1/\tau$ . Furthermore, it should be noted that we used two prime numbers to reduce the magnitude of possible resonances. Also, operating the galvanometer at higher frequencies (>300 Hz) may reduce its longevity.

### 4.2 Amplitude of galvanometer agitation

To find the optimum amplitude, we kept the frequencies of two channels constant for all fibres and varied the amplitude using a voltage generator from 1 to 140 mV in steps of 20 mV for SI50, GI50, and GI50t, and from 1 to 40 mV in steps of 5 mV for SI10. The variation of RMSE with amplitude is shown in Fig. 6. It is evident from Fig. 6 that the RMSE decreases i.e. modal noise reduces with applied amplitude up to 20 mV for SI10 and 60 mV for all the other fibres. The modal noise and RMSE increase if the amplitude exceeds these values. Moreover, in the process of minimizing RMSEs, we also lost photons due to the motion of the two mirrors. These motions cause an increase in focal spot size of the galvanometer output beam. The enlargement of spot size depends on the voltage applied. From our measurement (see Section 3.1), we found that the spot size would be about 84  $\mu\text{m}$  when 60 mV voltage was applied to each of the mirrors. As this is larger than the core diameter, the overall throughput of the instrument reduces. From the colour bar of Fig. 6, the amount of loss at the RMSE minima is found to be about 30 per cent of the peak counts for SI50 and GI50, 50 per cent for SI10, and 5 per cent for GI50t. Thus, we can improve the RMSEs but with

<sup>3</sup><https://github.com/indiajoe/SpectrumExtractor>

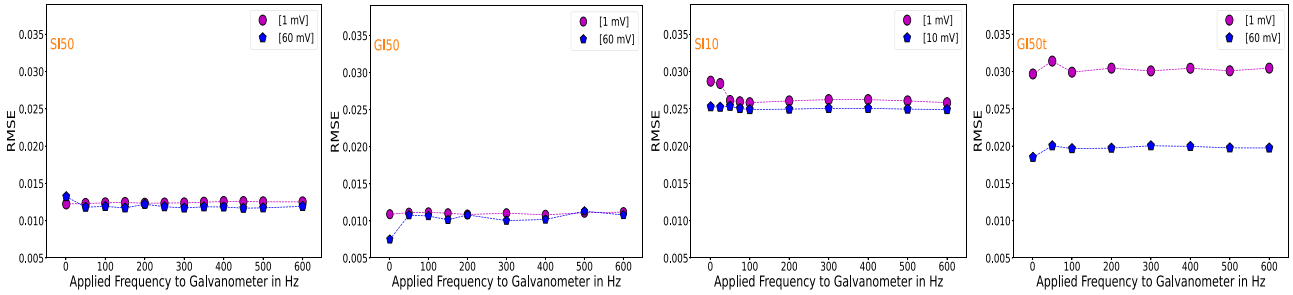


**Figure 5.** RMSE variation with applied frequencies to the galvanometer for different fibres (SI50, GI50, SI10, and GI50t, respectively) to find the optimum frequency for operating the galvanometer. We carried out our investigation for two amplitudes, 1 and 60 mV. The violet symbols correspond to 1 mV. The blue symbols represent 60 mV for SI50, GI50, and GI50t, and 10 mV for SI10 fibre. All plots are made on the same scale for relative comparison.

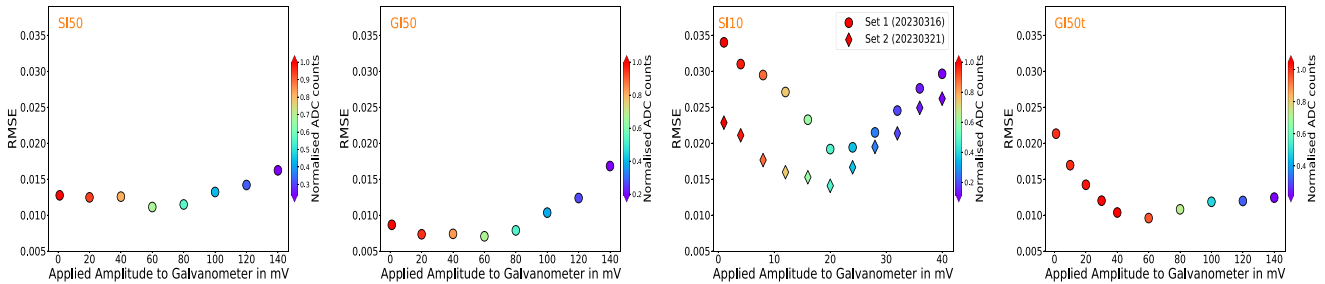


**Figure 6.** RMSE variation with applied amplitudes to the galvanometer for different fibres (SI50, GI50, SI10, and GI50t, respectively) to find the preferred amplitude for operating the galvanometer. The applied frequencies were 89 and 97 Hz to CH 1 and CH 2 of the frequency generator, respectively. The colour bar represents the normalized Analog-to-Digital Converter (ADC) counts corresponding to each RMSE measurement. See the text for details. All plots are made on the same scale for relative comparison.

a significant light-loss penalty in all fibres except GI50t. Therefore, there is a trade-off between reducing the RMSE and losing the light for most fibres tested. To further our investigation, we obtained data at two amplitudes (15 and 25 mV for SI10, and 20 and 60 mV for other fibres) as discussed in the following section.

#### 4.3 Investigating the efficiency of the galvanometer in mitigating modal noise

Once the optimum frequency and the operating amplitude of the galvanometer were set as previously described, we tested the effectiveness of our technique for all four fibres. We carried out our investigation 10 times and between each observation the state of the fibre (Fibre 2) was altered. In order to alter the state of the fibre and consequently the mode pattern, we altered the fibre position and also manipulated the fibre by stretching, squeezing, and twisting it. By doing this, we aimed to replicate all potential states of the fibre that might occur during actual sky observation in our laboratory setting. After changing the fibre state, we waited for 5 min before starting the exposure. Our results are displayed in Fig. 7. For SI50 and GI50, there is no notable change in RMSEs between the ‘GAL OFF’ and ‘GAL ON’ conditions. This could be due to several potential factors. For instance, SI50 and GI50 have a relatively high number of modes. Thus at any state of the fibre, the pattern of the modes is averaged out and we see less effect of modal noise on the spectra. In addition, we adopted the RMSE measurement to quantify the modal noise and our method seems to be insensitive to differentiating the modal noise between the ‘GAL OFF’ and ‘GAL ON’ conditions for these fibres. For GI50t, the RMSEs reduce significantly in the ‘GAL ON’ condition in comparison to the ‘GAL OFF’ condition.

The modal noise is found to be suppressed by around 60 per cent on average in the case of 60 mV amplitude of the applied voltage. In addition, we derived SNRs of the white light spectrum for 10 different cases as described above for GI50t in ‘GAL OFF’ and ‘GAL ON’ (with 60 mV) conditions following Stoehr et al. (2008). We found an improvement of SNR of about 4 per cent on average for ‘GAL ON’. An improvement of SNR implies less modal noise. For SI10, RMSEs are randomly distributed for the ‘GAL OFF’ and ‘GAL ON’ conditions for different observations. This could be due to the fact that the fibre is not relaxed during acquiring the data. More on fibre relaxation is discussed later in this paper (Section 4.5). The extracted spectra in ‘GAL OFF’ and ‘GAL ON’ conditions for various fibres are shown in Fig. 8. Comparing the spectra, significant mitigation of modal noise as well as a more symmetric modal noise pattern is seen.

#### 4.4 Fibre images with ‘GAL OFF’ and ‘GAL ON’

To demonstrate the effectiveness of the galvanometer further, we acquired images of the spatial distribution of light through our adopted fibres in ‘GAL OFF’ and ‘GAL ON’ conditions. For our experiment, we made a set-up for the microscope optical system, where a 20x objective and a ZWO ASI camera were implemented as laid out in Fig. 9. A 635 nm red laser was used to illuminate the fibre. The complete experimental set-up is similar to Fig. 1 except the spectrograph (rectangular box) is replaced by the microscope. The galvanometer is operated at the optimum voltage and amplitude for various fibres at the ‘GAL ON’ condition as mentioned in Sections 4.1 and 4.2. The exposure times were 0.5 s for SI10 and 0.04 s for all other fibres. The images of the near-field speckle pattern for different

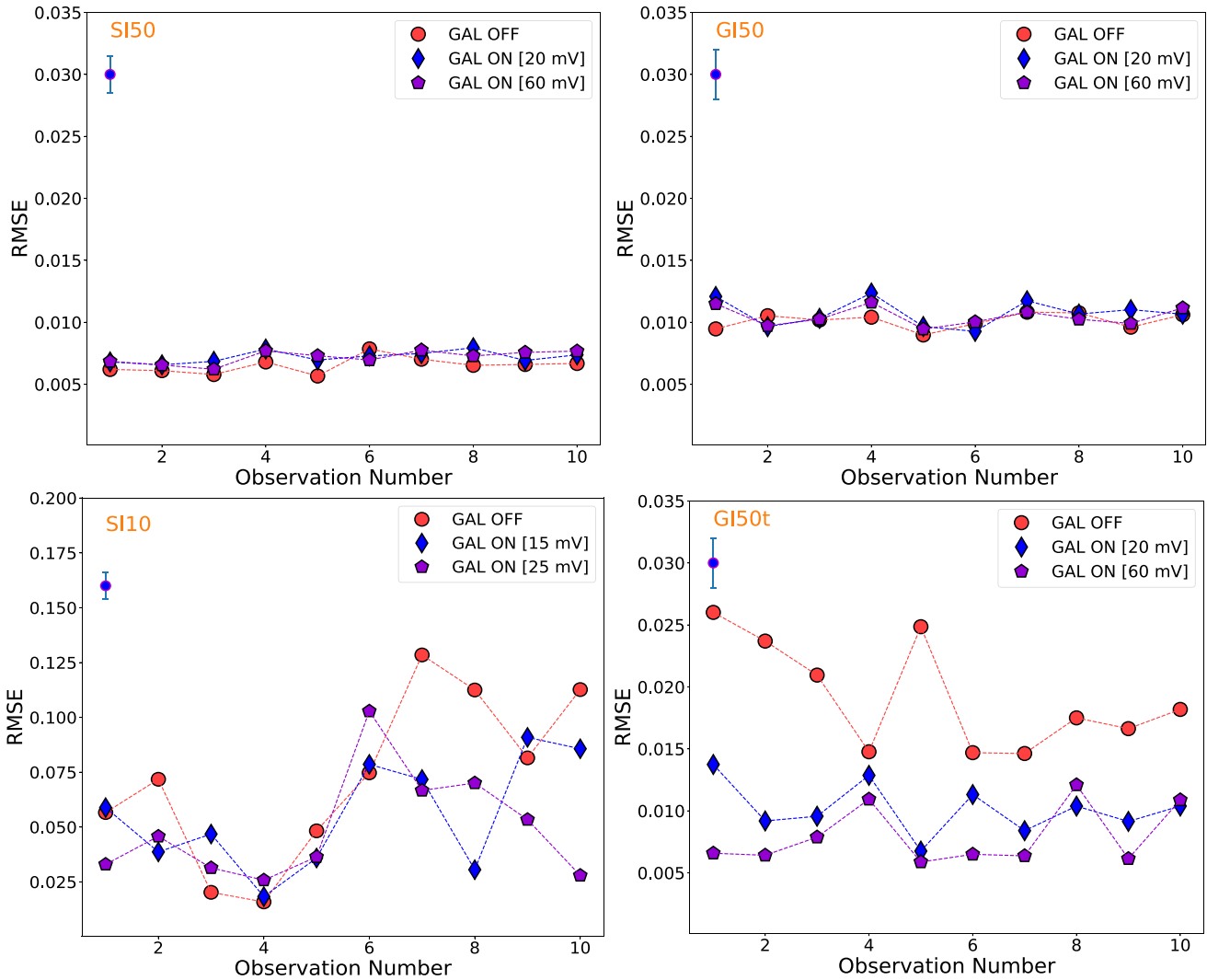


**Figure 7.** RMSE scatter with and without galvanometer for different fibres (SI50, GI50, SI10, and GI50t, respectively). The circular symbols represent the ‘GAL OFF’ condition. The other symbols correspond to the ‘GAL ON’ condition. Error bar at the top of each plot represents typical RMSE measurement error. We carried out our experiments for amplitudes, 20 mV (diamond symbols) and 60 mV (pentagon symbols) for SI50, GI50, and GI50t, and 15 mV (diamond symbols) and 25 mV (pentagon symbols) for SI10. The applied frequencies were 89 and 97 Hz to CH 1 and CH 2 of the frequency generator, respectively. We repeated the experiments multiple times to confirm our results. In each observation, the position of the fibre was altered to make sure that the state of the fibre (mode pattern) was not the same, and then we waited for 5 min before taking the data. GI50, SI50, and GI50t are made on the same scale for relative comparison.

fibres are displayed in Fig. 10. Fig. 10 clearly shows that the addition of the galvanometer significantly improves the speckle uniformity. We note, however, a relatively high background for GI50t. This effect could possibly be due to the fact that cladding mode suppression for other fibres was much better than the tapered fibre used for this test.

#### 4.5 Fibre relaxation

We extended our investigation further to explore the effect of fibre relaxation for SI10. The variation of RMSE with time for three different cases is shown in Fig. 11. For the first case (‘Undisturbed’, blue circles), the fibre was connected between the white light source and the spectrograph and allowed to rest overnight. No notable change in RMSE values with time was evident in this case. As the fibre was rested overnight, it can be considered to be in a relaxed condition, and thus, there is no distinct change in mode distribution between exposures. In the second case (‘Disturbed1’,

orange symbols), the fibre was disconnected from and reconnected to the fibre coupler of the white light source. Change in RMSE values were apparent in comparison to the former case. However, the variation of RMSE with time was insignificant. The reason for the change is probably due to the redistribution of modes because of the change in fibre coupling and external disturbance. In the third case (Disturbed2, green markers), the fibre was stretched along its length and then allowed to relax in the same condition. In this case, the RMSE was found to change significantly with time for the first 50 min. After 50 min, the change is insignificant. As the experiment was carried out in a general purpose temperature controlled laboratory environment, large temperature variations can be ruled out as a major contributor. Therefore, we believe that small stresses and strains due to externally applied forces are the reason for these changes. When the fibre was stretched, the applied external force disrupts the mechanical equilibrium in the fibre and as a result, the RMSE value increases. When the fibre was allowed to relax, it tends to

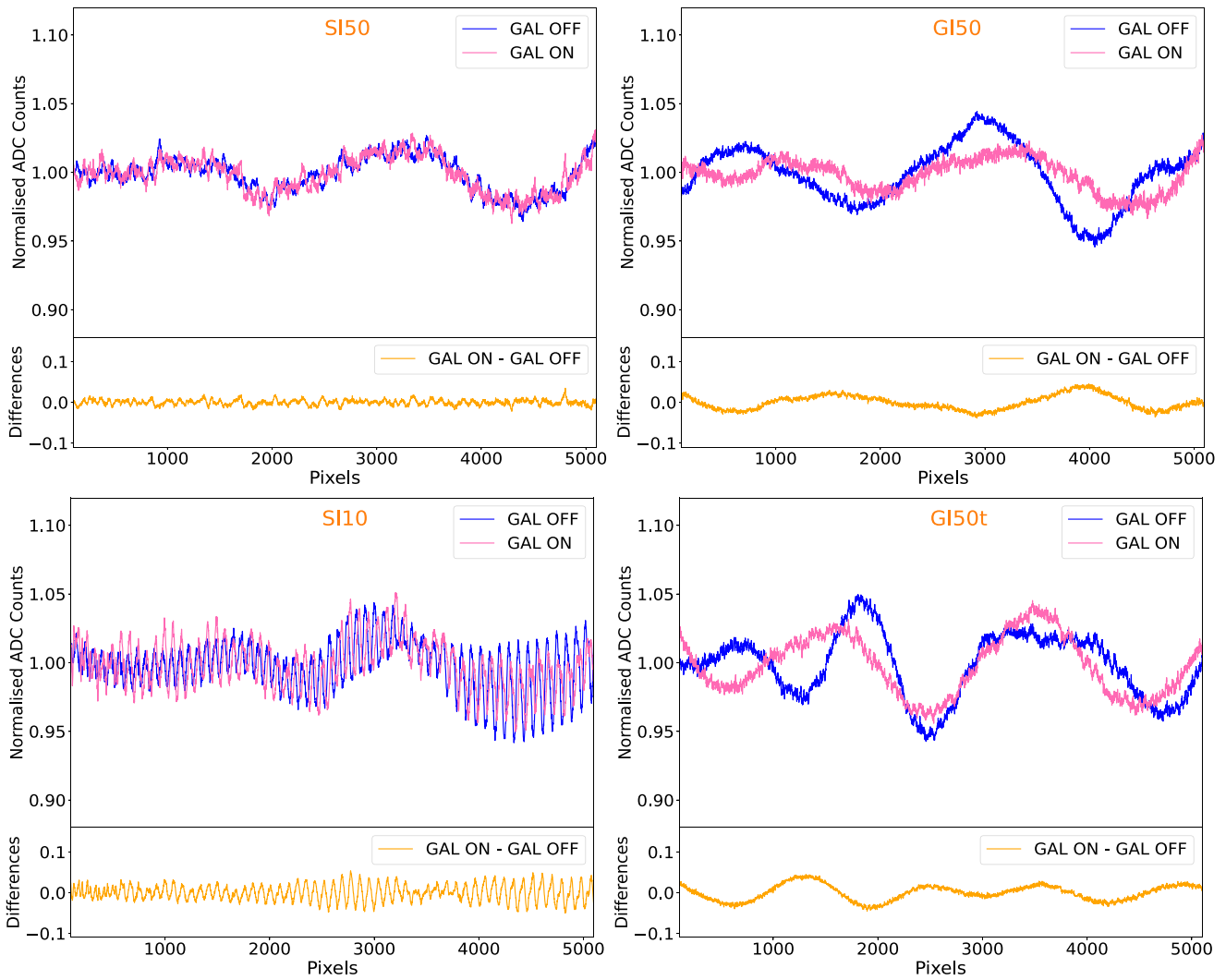


**Figure 8.** Extracted white light spectra of an order in GAL OFF and GAL ON conditions for different fibres (SI50, GI50, SI10, and GI50t, respectively). Applied frequencies to the voltage generator were 89 and 97 Hz to CH 1 and CH 2, respectively. The applied amplitude to the voltage generator was 15 mV for SI10 and 60 mV for other fibres. The spectral regime from 100 to 5000 pixels was considered for our analysis. Comparing spectrum in GAL OFF and GAL ON conditions, we can see that the spectrum are flatter when the galvanometer is on. The flat spectrum indicates the suppression of the modal noise.

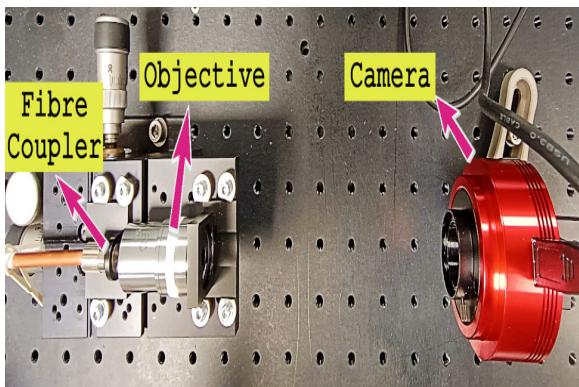


**Figure 9.** Illustration of microscope system set-up for imaging the spatial distribution of fibres modes.

back to an unstressed and unstrained state at room temperature and so RMSE decreases. However, the final relaxed state and hence the propagating mode patterns depends on the incident electric field, wavelength, fibre stresses and strains (Minardi et al. 2021). The observed variation of RMSE over time in the case of Disturbed2 might not be as prominent in fibres with a large core. Due to the large number of modes, the mode pattern tends to average out quickly. It is important to note that for small core fibre such as 10  $\mu\text{m}$  fibre, it is crucial to exercise additional caution against the movement of the fibre during the experiment. Additional experiments are required to fully understand this effect. Recent studies showed that thermal and mechanical stabilization of an MM fibre can greatly improve its' long-term stability (Redding et al. 2014; Liew et al. 2016; Cao et al. 2023). Furthermore, the most satisfactory explanation of our galvanometer-based modal noise mitigation method and fibre relaxation might be obtained using a complex wave-optics simulation



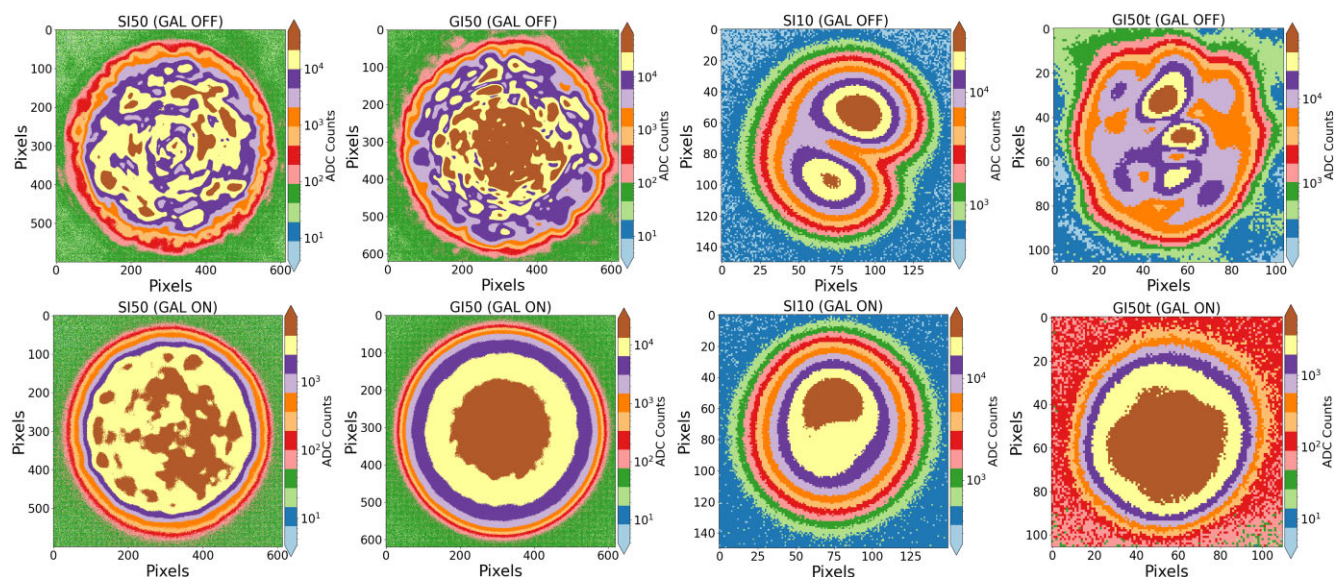


**Figure 10.** Comparison of images of the spatial distribution of light in various fibres in ‘GAL OFF’ (top panel) and ‘GAL ON’ (bottom panel). Applied frequencies to the voltage generator were 89 and 97 Hz to CH 1 and CH 2, respectively. The applied amplitude to the voltage generator was 60 mV (15 mV for SI10). It is evident that the mode pattern is averaged out greatly in the ‘GAL ON’ condition.

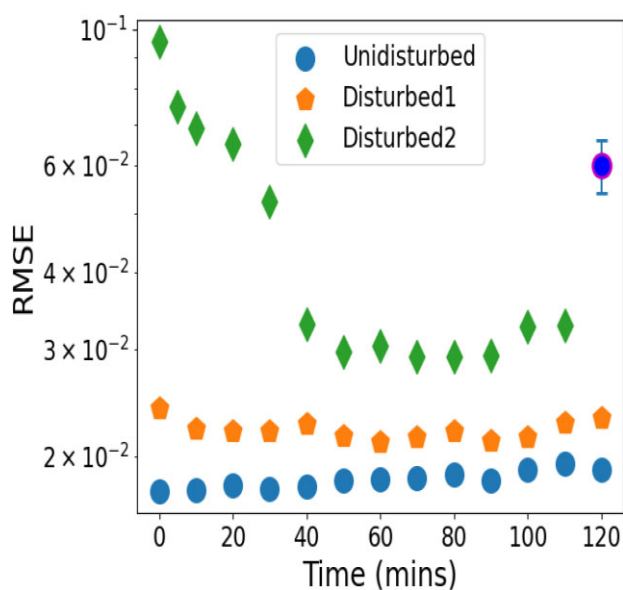


**Figure 11.** Variation of RMSE with Time to test the fibre relaxation for SI10 with ‘GAL OFF’ condition’. The RMSE variation for three states of the fibre is presented. In the first case (circular symbols), the fibre was connected from the white light source to the spectrograph and allowed to rest overnight. This state of the fibre is labelled as ‘Undisturbed’. In the second case (pentagon symbols, ‘Disturbed1’), the position of the fibre was altered by a small amount i.e. the fibre was disconnected from the fibre coupler of the white light source and reconnected. In the third case (diamond symbols), the fibre was stretched along its length and allowed to relax at the same position. This state of the fibre was termed ‘Disturbed2’. It is evident that the RMSE value decreases with time representing the stabilization of the mode pattern. Error bar at the top represents typical RMSE measurement error.

model such as COMSOL.<sup>4</sup> For such calculations, we need to treat each mode of the fibre independently with random variations of phases and mode patterns. Therefore, the model calculation will be computationally expensive with significant computer time. Thus, the detailed theoretical study is beyond the scope of this paper.

## 5. SUMMARY

In this paper, we have demonstrated the use of commercial off-the-shelf components to mitigate modal noise for fibre-fed high-resolution spectrographs. Our method uses a galvanometer designed to randomize the mode distribution while the light passes through it. The galvanometer uses two motorized rotating flat mirrors to mix the modes. The mode mixing can be controlled by setting up the frequency and amplitude of the applied sinusoidal signal through a voltage generator connected to each of the mirrors. To carry out our experiment, we used four different fibres: 50  $\mu\text{m}$  SI, 50  $\mu\text{m}$  GI, 10  $\mu\text{m}$  SI, and a combination of 50  $\mu\text{m}$  GI and 5:1 tapered fibre. We obtained white light spectra using a high-resolution spectrograph for our experiment and used RMSE measurement as a proxy for modal noise quantification. We first investigated the optimal frequency and amplitude of signal applied for efficient operation of the galvanometer. No significant frequency dependence on RMSE values was seen. However, the amplitude of the signal applied to the galvanometer did affect the RMSE and we used our measurement to find the optimum amplitude and maximize the galvanometer’s efficiency. Once the frequency and amplitude conditions were found, we repeated our experiment multiple times both with and without agitation by the galvanometer and showed that our technique was capable of mitigating modal noise efficiently. Among all the tested

<sup>4</sup><https://uk.comsol.com/>

fibres, the GI fibre combined with the tapered fibre (GI50t) was found to mitigate modal noise on an average by 60 per cent with a output light-loss penalty of only 5 per cent. In addition, we obtained images of the mode distribution for all fibres both with and without galvanometer agitation. We found that the use of a galvanometer significantly improves the uniformity of light illumination at the fibre output. Our technique offers benefits over other methods because of its simplicity, cost-effectiveness, and ease of implementation. We do not need to move the fibre during the observation. Thus, our methods is free from any mechanical agitation. It also does not compromise the lifetime of the fibre which might be the case if intense mechanical agitation methods are employed. However, there is a trade-off between improvement in modal noise and loss of light which limits the performance of the galvanometer and the throughput efficiency of the spectrograph. Additionally, we found that stressing the fibre with an external force can destabilize the spatial distribution of modes especially in small core fibres such as 10  $\mu\text{m}$  SI fibre. It takes a significantly long time ( $\sim 1$  h) for the fibre to return to a relaxed state. Therefore, such fibres need to be handled very carefully when used for spectroscopic observations.

## ACKNOWLEDGEMENTS

The authors are thankful to the reviewers for their critical and valuable comments on the original version of the manuscript, which helped us to improve the paper. We are very grateful to Tim Birks at University of Bath for his support in construction and supply of custom GI50t fibre. We are thankful for support of this research work through Newton fund grants from STFC under project identification number ST/P005667/1, ST/R006598/1, and ST/T007311/1.

## DATA AVAILABILITY

The data underlying this article will be shared on reasonable request to the corresponding author.

## REFERENCES

- Allen L. E. et al., 2018, American Astronomical Society Meeting Abstracts, #231, 246.08
- Artigau É. et al., 2014, in Ramsay S. K., McLean I. S., Takami H., eds, Proc. SPIE Conf. Ser. Vol. 9147, Ground-based and Airborne Instrumentation for Astronomy V. SPIE, Bellingham, p. 914715
- Avila G., 1988, in Barden S. C., ed., ASP Conf. Ser. Vol. 3, Fiber Optics in Astronomy. Astron. Soc. Pac., San Francisco, p. 63
- Baudrand J., Walker G. A. H., 2001, *PASP*, 113, 851
- Birks T. A., Gris-Sánchez I., Yerolatsitis S., Leon-Saval S. G., Thomson R. R., 2015, *Adv. Opt. Photonics*, 7, 107
- Blake C., Johnson J., Plavchan P., Sliski D., Wittenmyer R. A., Eastman J. D., Barnes S., 2015, American Astronomical Society Meeting Abstracts, #225, 257.32
- Bouchy F. et al., 2017, *The Messenger*, 169, 21
- Cao H., Čížmár T., Turtaev S., Tyc T., Rotter S., 2023, *Adv. Opt. Photonics*, 15, 524
- Chakraborty A. et al., 2014, *PASP*, 126, 133
- Choochalem P., Martin W. E., Jones H. R., Errmann R., Yerolatsitis S., Wright T. A., Buisset C., 2021, *Opt. Fiber Technol.*, 66, 102632
- Choochalem P., Martin W. E., Jones H. R., Usher S., Wright T. A., Yerolatsitis S., 2023, *Opt. Fiber Technol.*, 75, 103140
- Crepp J. R., 2014, *Science*, 346, 809
- Crepp J. R. et al., 2016, in Evans C. J., Simard L., Takami H., eds, Proc. SPIE Conf. Ser. Vol. 9908, Ground-based and Airborne Instrumentation for Astronomy VI. SPIE, Bellingham, p. 990819
- Epworth R., 1978, Proc. 4th European Conference on Optical Communications (ECOC). p. 492
- Fischer D. A. et al., 2016, *PASP*, 128, 066001
- Floris S. J., de Hon B. P., Bolhaar T., Smink R. W., 2020, *Opt. Fiber Technol.*, 54, 102116
- Halverson S., Roy A., Mahadevan S., Ramsey L., Levi E., Schwab C., Hearty F., MacDonald N., 2015a, *ApJ*, 806, 61
- Halverson S., Roy A., Mahadevan S., Schwab C., 2015b, *ApJ*, 814, L22
- Hill K. O., Tremblay Y., Kawasaki B. S., 1980, *Opt. Lett.*, 5, 270
- Hunter T. R., Ramsey L. W., 1992, *PASP*, 104, 1244
- Ishizuka M., Kotani T., Nishikawa J., Kurokawa T., Mori T., Kokubo T., Tamura M., 2018, *PASP*, 130, 065003
- Jones H. R. A., Martin W. E., Anglada-Escudé G., Errmann R., Campbell D. A., Baker C., Boonsri C., Choochalem P., 2021, *PASP*, 133, 025001
- Kawinkij A. et al., 2019, in Hull T. B., Kim D. W., Hallibert P., eds, Proc. SPIE Conf. Ser. Vol. 11116, Astronomical Optics: Design, Manufacture, and Test of Space and Ground Systems II. SPIE, Bellingham, p. 111161G
- Leon-Saval S. G., Birks T. A., Bland-Hawthorn J., Englund M., 2005, *Opt. Lett.*, 30, 2545
- Lhospipe E. et al., 2019, in Proc. SPIE Conf. Ser. Vol. 11117, Techniques and Instrumentation for Detection of Exoplanets IX. SPIE, Bellingham, p. 111170Z
- Liew S. F., Redding B., Choma M. A., Tagare H. D., Cao H., 2016, *Opt. Lett.*, 41, 2029
- McCoy K. S., Ramsey L., Mahadevan S., Halverson S., Redman S. L., 2012, in McLean I. S., Ramsay S. K., Takami H., eds, Proc. SPIE Conf. Ser. Vol. 8446, Ground-based and Airborne Instrumentation for Astronomy IV. SPIE, Bellingham, p. 84468J
- Mahadevan S. et al., 2012, in McLean I. S., Ramsay S. K., Takami H., eds, Proc. SPIE Conf. Ser. Vol. 8446, Ground-based and Airborne Instrumentation for Astronomy IV. SPIE, Bellingham, p. 84461S
- Mahadevan S., Halverson S., Ramsey L., Venditti N., 2014, *ApJ*, 786, 18
- Mayor M. et al., 2003, *The Messenger*, 114, 20
- Mégevand D. et al., 2012, in McLean I. S., Ramsay S. K., Takami H., eds, Proc. SPIE Conf. Ser. Vol. 8446, Ground-based and Airborne Instrumentation for Astronomy IV. SPIE, Bellingham, p. 84461R
- Mickelson A. R., Weierholt A., 1983, *Appl. Opt.*, 22, 3084
- Minardi S., Harris R. J., Labadie L., 2021, *A&AR*, 29, 6
- Monerie M., Jeunhomme L., 1980, *Opt. Quantum Electron.*, 12, 449
- Oliva E., Rainer M., Tozzi A., Sanna N., Iuzzolino M., Brucalassi A., 2019, *A&A*, 632, A21
- Petersburg R. R., McCracken T. M., Eggerman D., Jurgenson C. A., Sawyer D., Szymkowiak A. E., Fischer D. A., 2018, *ApJ*, 853, 181
- Pike F. A., Benoît A., MacLachlan D. G., Harris R. J., Gris-Sánchez I., Lee D., Birks T. A., Thomson R. R., 2020, *MNRAS*, 497, 3713
- Quirrenbach A. et al., 2012, in McLean I. S., Ramsay S. K., Takami H., eds, Proc. SPIE Conf. Ser. Vol. 8446, Ground-based and Airborne Instrumentation for Astronomy IV. SPIE, Bellingham, p. 84460R
- Ramsay L. W., 1988, in Barden S. C., ed., ASP Conf. Ser. Vol. 3, Fiber Optics in Astronomy. Astron. Soc. Pac., San Francisco, p. 26
- Raskin G., Rogozin D., Mladenov T., Schwab C., Coutts D., 2020, in Ellis S. C., d'Orgeville C., eds, Proc. SPIE Conf. Ser. Vol. 11203, Advances in Optical Astronomical Instrumentation 2019. SPIE, Bellingham, p. 1120310
- Redding B., Alam M., Seifert M., Cao H., 2014, *Optica*, 1, 175
- Roy A., Halverson S., Mahadevan S., Ramsey L. W., 2014, in Ramsay S. K., McLean I. S., Takami H., eds, Proc. SPIE Conf. Ser. Vol. 9147, Ground-based and Airborne Instrumentation for Astronomy V. SPIE, Bellingham, p. 91476B
- Schwab C. et al., 2016, in Evans C. J., Simard L., Takami H., eds, Proc. SPIE Conf. Ser. Vol. 9908, Ground-based and Airborne Instrumentation for Astronomy VI. SPIE, Bellingham, p. 99087H
- Seifahrt A., Stürmer J., Bean J. L., Schwab C., 2018, in Evans C. J., Simard L., Takami H., eds, Proc. SPIE Conf. Ser. Vol. 10702, Ground-based and Airborne Instrumentation for Astronomy VII. SPIE, Bellingham, p. 107026D

- Spronck J. F. P., Fischer D. A., Kaplan Z. A., Schwab C., 2012, in McLean I. S., Ramsay S. K., Takami H., eds, Proc. SPIE Conf. Ser. Vol. 8446, Ground-based and Airborne Instrumentation for Astronomy IV. SPIE, Bellingham, p. 84468Z
- Spronck J. F. P., Fischer D. A., Kaplan Z. A., Schwab C., Szymkowiak A., 2013, *PASP*, 125, 511
- Spronck J. F. P., Fischer D. A., Kaplan Z., Jurgenson C. A., Valenti J., Moriarty J., Szymkowiak A. E., 2015, *PASP*, 127, 1027
- Stoehr F. et al., 2008, in Argyle R. W., Bunclark P. S., Lewis J. R., eds, ASP Conf. Ser. Vol. 394, Astronomical Data Analysis Software and Systems XVII. Astron. Soc. Pac., San Francisco, p. 505
- Yerolatsitis S., Harrington K., Birks T. A., 2017, *Opt. Express*, 25, 18713

## SUPPORTING INFORMATION

Supplementary data are available at *RASTAI* online.

### **ModalNoisePaper-rastiV\_final.zip**

Please note: Oxford University Press is not responsible for the content or functionality of any supporting materials supplied by the authors. Any queries (other than missing material) should be directed to the corresponding author for the article.

This paper has been typeset from a  $\text{\TeX/L\AA\TeX}$  file prepared by the author.